Fermilab FERMILAB-Pub-03/179-E July 2003

Search for Rare and Forbidden 3-body Di-muon Decays of the Charmed Mesons D^+ and D_s^+

The FOCUS Collaboration ⋆

J. M. Link [a] P. M. Yager [a] J. C. Anjos [b] I. Bediaga [b] C. Göbel [b]
J. Magnin [b] A. Massafferri [b] J. M. de Miranda [b] I. M. Pepe [b]
E. Polycarpo [b] A. C. dos Reis [b] S. Carrillo [c] E. Casimiro [c]
E. Cuautle [c] A. Sánchez-Hernández [c] C. Uribe [c] F. Vázquez [c]
L. Agostino [d] L. Cinquini [d] J. P. Cumalat [d] B. O'Reilly [d]
I. Segoni [d] M. Wahl [d] J. N. Butler [e] H. W. K. Cheung [e]
G. Chiodini [e] I. Gaines [e] P. H. Garbincius [e] L. A. Garren [e]
E. Gottschalk [e] P. H. Kasper [e] A. E. Kreymer [e] R. Kutschke [e]
M. Wang [e] L. Benussi [f] L. Bertani [f] S. Bianco [f] F. L. Fabbri [f]
A. Zallo [f] M. Reyes [g] C. Cawlfield [h] D. Y. Kim [h] A. Rahimi [h]
J. Wiss [h] R. Gardner [i] A. Kryemadhi [i] Y. S. Chung [j] J. S. Kang [j]
B. R. Ko [j] J. W. Kwak [j] K. B. Lee [j] K. Cho [k] H. Park [k]
G. Alimonti [ℓ] S. Barberis [ℓ] M. Boschini [ℓ] A. Cerutti [ℓ]
P. D'Angelo [ℓ] M. DiCorato [ℓ] P. Dini [ℓ] L. Edera [ℓ] S. Erba [ℓ]
M. Giammarchi [ℓ] P. Inzani [ℓ] F. Leveraro [ℓ] S. Malvezzi [ℓ]
D. Menasce [ℓ] M. Mezzadri [ℓ] L. Moroni [ℓ] D. Pedrini [ℓ]
C. Pontoglio [ℓ] F. Prelz [ℓ] M. Rovere [ℓ] S. Sala [ℓ]
T. F. Davenport III [m] V. Arena [n] G. Boca [n] G. Bonomi [n]
G. Gianini [n] G. Liguori [n] D. Lopes Pegna [n] M. M. Merlo [n]
D. Pantea [n] S. P. Ratti [n] C. Riccardi [n] P. Vitulo [n]
H. Hernandez [o] A. M. Lopez [o] E. Luiggi [o] H. Mendez [o] A. Paris [o]
J. Quinones [o] J. E. Ramirez [o] W. A. Rolke [o] Y. Zhang [o]
J. R. Wilson [p] T. Handler [q] R. Mitchell [q] D. Engh [r] M. Hosack [r]
W. E. Johns [r] M. Nehring [r] P. D. Sheldon [r] K. Stenson [r]
E. W. Vaandering [r] M. Webster [r] M. Sheaff [s]

[a] *University of California, Davis, CA 95616*

[b] *Centro Brasileiro de Pesquisas Físicas, Rio de Janeiro, RJ, Brasil*

[c] *CINVESTAV, 07000 México City, DF, Mexico*

[d] *University of Colorado, Boulder, CO 80309*
[e] *Fermi National Accelerator Laboratory, Batavia, IL 60510*
[f] *Laboratori Nazionali di Frascati dell'INFN, Frascati, Italy I-00044*
[g] *University of Guanajuato, 37150 Leon, Guanajuato, Mexico*
[h] *University of Illinois, Urbana-Champaign, IL 61801*
[i] *Indiana University, Bloomington, IN 47405*
[j] *Korea University, Seoul, Korea 136-701*
[k] *Kyungpook National University, Taegu, Korea 702-701*
[ℓ] *INFN and University of Milano, Milano, Italy*
[m] *University of North Carolina, Asheville, NC 28804*
[n] *Dipartimento di Fisica Nucleare e Teorica and INFN, Pavia, Italy*
[o] *University of Puerto Rico, Mayaguez, PR 00681*
[p] *University of South Carolina, Columbia, SC 29208*
[q] *University of Tennessee, Knoxville, TN 37996*
[r] *Vanderbilt University, Nashville, TN 37235*
[s] *University of Wisconsin, Madison, WI 53706*

Abstract

Using a high statistics sample of photo-produced charm particles from the FOCUS experiment at Fermilab, we report results of a search for eight rare and Standard-Model-forbidden decays: $D^+,\ D_s^+ \to h^\pm\mu^\mp\mu^+$ (with $h = \pi, K$). Improvement over previous results by a factor of 1.7–14 is realized. Our branching ratio upper limit $D^+ \to \pi^+\mu^-\mu^+$ of 8.8×10^{-6} at the 90% C.L. is below the current MSSM R-Parity violating constraint.

1 Introduction

The search for rare and forbidden decays of charm particles is enticing since Standard Model (SM) predictions for interesting decays tend to be beyond the reach of current experiments, and a signal is an indication of unexpected physics.

Standard Model predictions [1–3] for the branching ratios of rare decays $D^+, D_s^+ \to h^+\mu^-\mu^+$ (with $h = \pi, K$) are dominated by long range effects which are notoriously difficult to calculate. Even so, the differences between the three predictions in [1–3], although using individual treatments for the

* See http://www-focus.fnal.gov/authors.html for additional author information.

decay spectra, are quite manageable. For example, the predicted integrated rate for $D^+ \to \pi^+\mu^-\mu^+$ varies by only a factor of 2 while the experimental limits are a factor of 5–10 away. Minimal Supersymmetric Standard Model (MSSM) R-Parity violating extensions can significantly increase this rate. Experimental results for $D^+ \to \pi^+\mu^-\mu^+$ currently set the best constraint for the product of the MSSM R-Parity violating couplings: $|\lambda'_{22k}\lambda_{21k}|' < 0.004$ [1]. Until experiments reach the SM limit for these rare decays, a signal indicates new physics or a needed refinement in the interpretation of the SM. Decays of the form $D^+,\ D_s^+ \to h^-\mu^+\mu^+$ (with $h = \pi, K$) are forbidden in the SM since they violate lepton number conservation, and a signal in these modes is direct evidence of new physics.

In this paper, we present new upper limits for the branching ratios of 3-body di-muonic decays of the D^+ and D_s^+ mesons mentioned above. Unless specifically mentioned, all results include a lower limit of 0 at the 90% C.L.. Our results represent a factor of 1.7–14 improvement over previous experimental limits [4,5]. The result for the branching ratio upper limits of $D^+ \to \pi^+\mu^+\mu^-$ of 8.8×10^{-6} @ 90% C.L. and $D_s^+ \to \pi^+\mu^+\mu^-$ of 2.6×10^{-5} @ 90% C.L. are both within a factor of 5 of the Standard Model (long range) predictions 1.9×10^{-6} [1] and 6.1×10^{-6} [2] respectively. The result for the branching ratio upper limit $D^+ \to \pi^+\mu^+\mu^-$ of 8.8×10^{-6} @ 90% C.L. is below the MSSM R-Parity violating constraint [1].

The data for this analysis were collected using the Wideband photoproduction experiment FOCUS during the 1996–1997 fixed-target run at Fermilab. The FOCUS detector is a large aperture, fixed-target spectrometer with excellent vertexing and particle identification used to measure the interactions of high energy photons on a segmented BeO target. The FOCUS beamline [6] and detector [7–10] have been described elsewhere.

2 Event Selection

We look for D's through the 3-body decay chains $D^+,\ D_s^+ \to h^\mp\mu^\pm\mu^+$ (where the h represents a pion or a kaon) for rare decays and $D^+ \to K^-\pi^+\pi^+$ or $D_s^+ \to K^-K^+\pi^+$ for normalization (charge conjugate modes are implied throughout this paper). In order to search for the set of cuts that provides signal optimization, we place initial (loose) requirements on the reconstructed data to produce a base sample, and then we place a series of (tighter) cuts on the base sample. The loose requirements consist of acceptance, momentum, vertexing, and particle identification cuts. Note that for all cuts, care is taken to ensure that the normalization modes receive the same cuts as the di-muon modes where possible.

Due to the finite lifetime and Lorentz boost of charm candidates, the primary interaction vertex and secondary decay vertex can have a significant separation along the beam direction. Secondary vertices are formed from 3 candidate tracks, and the resulting momentum vector of the 3 tracks is used as a seed to search for a primary vertex [7]. We require that the confidence level of the secondary vertex fit (DCL) exceed 1%, the confidence level of the primary vertex fit exceed 1%, the significance of separation between the primary and secondary vertices (ℓ/σ_ℓ) exceed 5, and the confidence level that any of the secondary tracks is consistent with the primary vertex (ISO1) be less than 10%. The latter cut is included to remove the contamination from D^{*+} decays and other tracks originating from the primary that could be confused with secondary tracks.

We use the Čerenkov system [8] to identify pions and kaons. For each track, $W_{\rm obs} = -2\log(\mathcal{L})$ is computed, where $\mathcal{L}$ is the likelihood that a track is consistent with a given particle hypothesis. For a candidate kaon, we require $W_{\rm obs}(\pi) - W_{\rm obs}(K)$ (kaonicity) be greater than 0.5. For a candidate pion in a rare mode, we require $W_{\rm obs}(K) - W_{\rm obs}(\pi)$ (pionicity) be greater than -15.

Muon candidates are required to be within the acceptance of either of the 2 muon systems in FOCUS [10]. We require the tracks in a normalizing mode corresponding to muon tracks in a rare decay mode be in the acceptance of one of the muon systems as well. Since the rate of muon misidentification increases at low momentum, we place a requirement that the momentum of "muon" tracks within the acceptance of the wide angle (outer) muon system ($P_\mu^{\rm outer}$) be greater than 6 GeV/c and those within the low angle (inner) muon system ($P_\mu^{\rm inner}$) be greater than 8 GeV/c. All muon candidates are required to have associated hits in either muon system sufficient to meet a minimum confidence level, μ_{CL}, of 1% for the muon hypothesis, and must pass additional muon cuts depending on the system traversed. For the outer muon system, muon candidates must traverse a minimum of 150 cm of material, produce hits in 2 of 3 planes of the detector, and these 2 (or more) hits (called a cluster) must not be shared by the other muon candidate. For the inner system, at least 4 of 6 planes of the detector must record hits consistent with the candidate track, no more than 2 of these hits can be shared with the other candidate muon track, and a fit to the hypothesis that the inner muon candidate track had the same measured momentum in both magnets traversed was required to exceed 1%. This last cut is used to reduce contamination from particles that decay and produce a muon as they traverse the spectrometer. This cut is also applied to the pions in the normalization modes, and the lowest momentum kaon, when possible, for the D_s^+ normalization mode. Finally, all other tracks in the event are fit to the muon hypothesis using the hits from a candidate muon, and the highest confidence level from the fits, ISO$_\mu$, is saved. No ISO$_\mu$ cut was required for the base sample, but a 10% ISO$_\mu$ is included in the set of cuts used for sensitivity optimization.

For the D_s^+ normalization signal, $D_s^+ \to K^+K^-\pi^+$, a cut was applied to reduce the reflection when one of the pions from $D^+ \to K^-\pi^+\pi^+$ is misidentified as a kaon. Under the hypothesis that the same sign D_s^+ kaon track is assumed to be pion, the invariant mass is calculated. If the new invariant mass is within 3 standard deviations of the D^+ mass, the kaonicity of the same sign kaon must exceed 6. Additionally, we require that the reconstructed K^+K^- invariant mass be within 3 standard deviations of the ϕ mass.

Our analysis methodology (Section 3) requires a base sample of events of sufficiently small size (150 events) for a reasonable processing time. Base samples were obtained by applying the minimum ℓ/σ_ℓ cut in the range of 5 to 8 which brought the sample size below 150. The series of cuts applied to these samples was arranged into a grid. This cut grid was based on kinematic variables, particle ID algorithm results, vertex quality, and event topology. For example, once the lower cut in ℓ/σ_ℓ was determined, the ℓ/σ_ℓ cut was allowed to vary in steps of 2 units up to a maximum of 21 or 22. The cuts used have been shown to be effective for other charm decays besides those presented in this analysis.

Since the kaonicity cut can be applied to the kaon modes identically, there is an inherent increase in the size of the cut grid when the pionicity cut is used for the pion modes. To keep the size of the cut grid roughly the same, and to prevent memory overflows in software that was difficult to modify, we reduced the size of the cut grid for the pion modes. The grid (see Table 1) includes cuts on ℓ/σ_ℓ, ISO1, DCL, kaonicity, pionicity, μ_{CL}, ISO_μ, and the momentum of muon candidates. The normalizing modes used to compute the branching ratios for D^+ and D_s^+ are shown in Figure 1 for the loosest cuts in the grid.

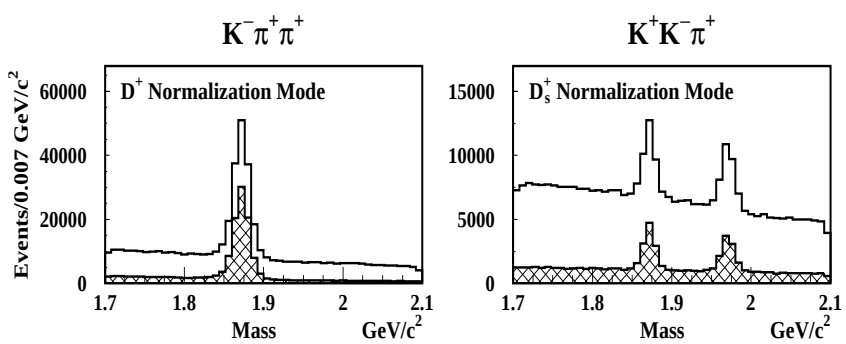

Fig. 1. Modes used to normalize the rare decay modes. The solid histograms represent the loosest cuts employed in the analysis, while the superimposed cross-hatched histograms represent data which has had the tightest cuts used in the analysis applied. Notice the large reduction in background relative to the signal for both the D^+ and the D_s^+ modes over the range of cuts used.

In order to perform signal optimizations, calculate efficiencies, and estimate yields, there is a distinction made between the signal region, where events for the desired mode are expected to occur, and the background sidebands, where

Table 1
Analysis cuts used in the cut grid. Variables are described in the text. The best cut on average represents a point on the cut grid used in a systematic check of our result that is described in the "Systematic Checks and Results" section of the paper. Cuts indicated by { } are applied only to the kaon modes to keep the cut grid about the same size for kaon and pion modes. Notice that the cuts removed for the pion modes are chosen either very far from the "Best Cut" (explained later in the text), or represent a small reduction in the stepping of a cut that varies logarithmically (ISO1).

Variable	Cut Values Used in the Grid	Best Cut on Average
ℓ/σ_ℓ	$> 5 \rightarrow 22$	> 13 (D^+), 10 (D_s^+)
ISO1	$< 0.1, \{0.03\}, 0.01, \{0.003\}, 0.001$	< 0.1
DCL	$> 1\%, 2\%, 4\%$	$> 1\%$ (D^+), 2% (D_s^+)
Kaonicity (kaon modes)	$> 0.5, 1.0, 2.0$	> 1.0
Pionicity (pion modes)	$> -15, -3, -1$	> -3
μ_{CL}	$> 1\%, 5\%, 10\%$	$> 5\%$
ISO_μ	$< 0.10, 1.0$	< 1.0
$\mathrm{P}_\mu^{\mathrm{inner}}$ (GeV/c)	$> 8, 9, 10, 11, 12, \{14\}$	> 9
$\mathrm{P}_\mu^{\mathrm{outer}}$ (GeV/c)	$> 6, 7, 8, 9, \{10\}$	> 7

the amount of signal is expected to be minimal. The background sidebands are used to estimate the amount of contamination in the signal region. We define the signal region to be within 2 standard deviations of the nominal reconstructed parent particle mass (i.e. either the D^+ ($\pm$ 20 MeV/c^2) or the D_s^+ ($\pm$ 18 MeV/c^2)) and the background region to be any invariant mass reconstructed outside the signal regions between 1.7 and 2.1 GeV/c^2. An exception is made for $D^+,\ D_s^+ \rightarrow K^-\mu^+\mu^+$. For $D^+ \rightarrow K^-\mu^+\mu^+$ the background sidebands are required to be between 1.75 and 2.1 GeV/c^2. This approximately splits the expected contribution of $D^+ \rightarrow K^-\pi^+\pi^+$, where the 2 pions are both mis–identified as muons, equally between signal and background regions. For $D_s^+ \rightarrow K^-\mu^+\mu^+$ we require the lower sideband to begin 2 standard deviations above the D^+ mass. This effectively removes the $D^+ \rightarrow K^-\pi^+\pi^+$ signal that comes from mis–identified muons. The centroid and standard deviation for each mode are determined by fitting the reconstructed parent particle mass in the normalization mode. Since there is a small shift in the mass centroid between data and Monte Carlo, we use the data to determine the regions for data and Monte Carlo to determine the regions for Monte Carlo.

The shape of the background in each rare mode is determined using a large sample of photoproduction Monte Carlo events where all charm species and known decay modes are simulated. The shape of the background is used to

determine τ, which is the ratio of the number of background events expected in the sideband region to the number of background events expected in the signal region. An average τ is computed for each mode from all the τ's in the cut grid for that particular mode. We find that the ratio of Monte Carlo efficiencies and τ are stable over the cut combinations in the grid, but we require at least 10 surviving Monte Carlo events to determine each τ used in the average to prevent variations due to low Monte Carlo statistics in the signal region.

These definitions are used in the determination of the branching ratio limits in the analysis described below.

3 Analysis

The analysis technique emphasized a careful approach to the treatment of backgrounds in a limited statistics analysis. The "blind" approach, to select cuts that optimize signal efficiency relative to background sidebands, may still lead to a downward fluctuation of the sidebands relative to the masked off "signal" region and a more conservative limit on average [11]. Further, authors frequently use the technique outlined by Feldman and Cousins [12] to calculate the confidence levels used in the calculation of their limits. The Feldman–Cousins approach does not explicitly include fluctuations of the background. Indeed, the Particle Data Group [13] suggests presenting a measure of the experimental sensitivity, defined as the average 90% confidence upper limit of an ensemble of experiments with the expected background and no true signal, in addition to the reported limit whenever experiments quote a result. None of the methods suggested in the PDG, including the Cousins–Highland method for including systematic errors in upper limits [14], properly deal with fluctuations in the background and bias in selecting the data.

For this analysis, we chose a method suggested by Rolke and Lopez [15] which includes the background fluctuations directly into the calculation of the likelihood. The composite Poisson probability of finding x events in a signal region and y events in background sidebands given a signal μ and a background b is:

$$P_{\mu,b}(x,y) = \frac{(\mu+b)^x e^{-(\mu+b)}}{x!} \; \frac{(\tau b)^y e^{-(\tau b)}}{y!} \tag{1}$$

where τ is the expected ratio of the number of background events in the sideband regions to the signal region. Rolke and Lopez have shown that including the second Poisson factor in this expression leads to confidence intervals with better coverage than those of Feldman–Cousins who only consider the first factor.

In a second paper Rolke and Lopez have shown that bias can also be introduced during the selection of optimal cuts [11]. If a single cut is chosen based partly on the level of background in the sidebands (as is typical), there is a tendency to optimize on downward fluctuations and, hence, to underestimate the background level in the signal region. The resultant limits from such an "optimized" analysis, even though carried out in a "blind" fashion, will not have the correct coverage.

In order to reduce the bias due to selection, Rolke and Lopez suggest the data be sampled using a "Dual Bootstrap" method. In a bootstrap, the experimentally observed data set of N events is used to create an ensemble of many different N-event experiments or data sets, obtained by random sampling of the original data set allowing repeated events. In the Dual Bootstrap, two independently bootstrapped data sets are created. One set is used to optimize the cuts which are then applied to the second set in order to calculate the confidence intervals. This procedure is repeated 10,000 times and the median value for the limits is the final result. The two bootstrap data sets are sufficiently independent that the background estimate from the second is very nearly unbiased.

We use the experimental sensitivity (see Eqn. 2 and Eqn. 3) as our figure of merit to optimize cuts. A matrix or grid of possible data quality selection cuts are applied to the first bootstrap data set. The point in the multidimensional cut grid which has the best (smallest) sensitivity is applied to the second bootstrap data set. Limits for the branching ratio and a new sensitivity are computed from this second set. The Dual Dootstrap procedure is shown schematically in Figure 2.

For a given τ with y sideband events, the average 90% confidence upper limit for the number of events in the signal region when there is no true signal, $S_\tau(y)$, can be calculated from the Rolke-Lopez [15] 90% upper limit table as:

$$S_\tau(y) = \sum_{x=0}^{\infty} U_\tau(x,y) \cdot P_{y/\tau}(x) \tag{2}$$

where $U_\tau(x,y)$ is the upper limit of the signal, and $P_{y/\tau}(x)$ is the Poisson probability of x when the expected background is y/τ.

The experimental sensitivity is:

$$\text{Sensitivity} = \text{BR}_{\text{norm}} \frac{S_\tau(y)}{Y_{\text{norm}}} \epsilon \tag{3}$$

where the branching ratio of the normalization mode, BR_{norm}, comes from the PDG [16], Y_{norm} is the yield of the normalization mode (determined from a

sideband subtraction), and ϵ is the ratio, determined using Monte Carlo, of the normalization mode efficiency divided by the rare decay mode efficiency. For different bootstrap data sets and different cut sets, y, τ, $Y_{\rm norm}$, $S_\tau(y)$, and ϵ can be different. The sensitivity meets the requirement of a blind analysis, i.e. it does not depend on the number of events observed in the signal region. In a Dual Bootstrap procedure one sensitivity is calculated as the best sensitivity for the first data set and a second (less-biased) sensitivity is calculated when the "best" cuts are applied to the second data set.

The 90% confidence upper limit for the rare branching ratio is:

$$\text{Upper Limit} = \text{BR}_{\rm norm}\frac{Y_{\rm rare}}{Y_{\rm norm}}\epsilon \tag{4}$$

where $Y_{\rm rare} = U_\tau(z, y)$ is the Rolke-Lopez 90% confidence upper limit for the signal yield given z events in the signal region. The lower limit has a similar expression.

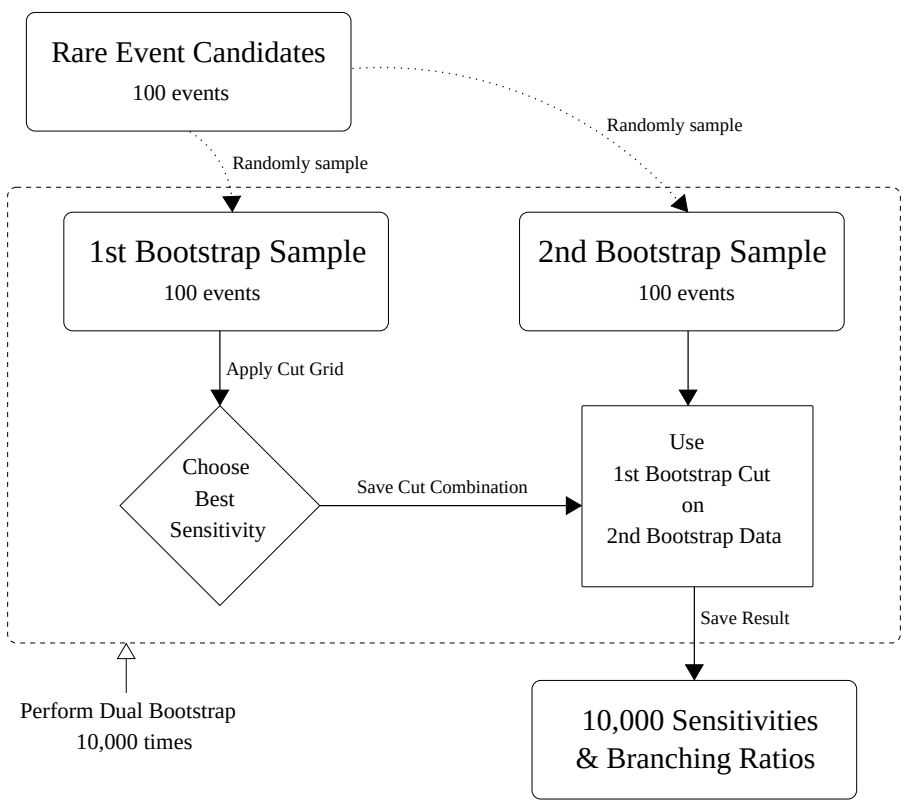

Fig. 2. A flowchart for the Dual Bootstrap on a sample size of 100 events. Note the parallel structure of the sampling with replacement that separates the cut selection that optimizes sensitivity from the calculation of the sensitivities and branching ratios used to determine the final result. Thus, only the data sidebands and the expectation of the shape of the background is used in the cut selection, even though events may be chosen from throughout the data set during the bootstrap process.

The salient features of parameters coming from the Dual Bootstrap analysis are illustrated in Figure 3 for the decay mode $D^+ \to \pi^+\mu^-\mu^+$. Several features are worth mentioning. The spread of the branching ratio upper limits is in general larger than the spread of the best sensitivities. This happens since the spread of the branching ratio upper limits is dominated by fluctuations in the signal region while the spread in the best sensitivities stems from the larger background region used in the estimate. This is a distinct advantage when determining τ with large sidebands rather than smaller sidebands where the fluctuations in the background can become more problematic. The single bootstrap sensitivities sample the very lowest end of the sensitivity spectra, and fluctuations often place the best bootstrap sensitivity below any calculated from the data directly. Notice though, that the second bootstrap sensitivities remove the bias and give a median sensitivity somewhat above the minimum expected by the data. This is a safeguard against choosing a single cut that produces an outlier or poor estimation of the true sensitivity. Thus, the Dual Bootstrap method allows us to optimize the sensitivity for *each* decay mode while retaining correct coverage. Also notice that the Dual Bootstrap branching ratio upper limits can cover a larger spread than the original branching ratio upper limits shown for all cut combinations. This can be understood if one realizes that for a small number of events in the signal region, the background can vary considerably in the second bootstrap, and the confidence interval calculation amplifies the effect, producing a larger spread.

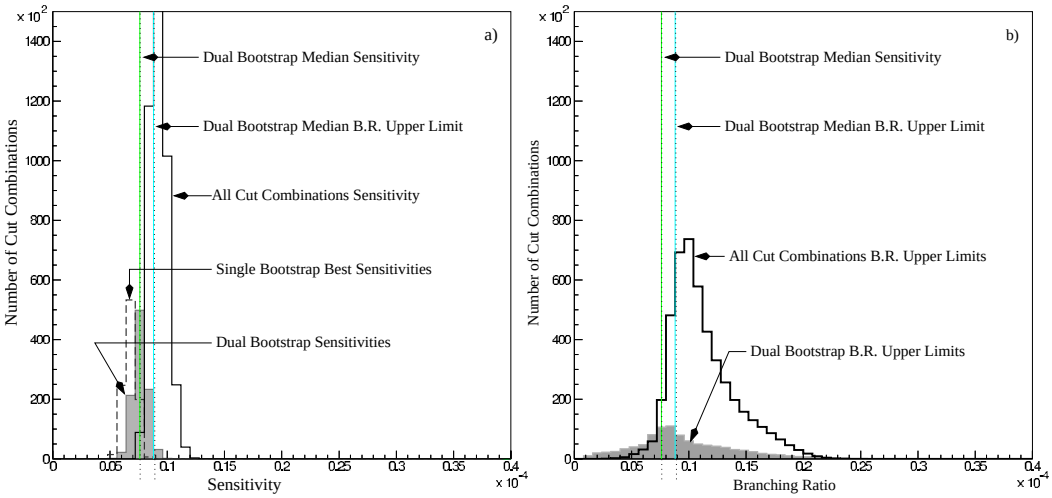

Fig. 3. The distribution of results used in the determination of the branching ratio confidence interval for the decay mode $D^+ \to \pi^+\mu^-\mu^+$. In plot a), the sensitivity distributions are shown, and in plot b) the branching ratio distributions are shown.

4 Systematic Checks and Results

The largest sources of systematic uncertainty in this analysis are estimated to come from uncertainties in the Monte Carlo simulation and uncertainty in the branching ratios used for the normalizing modes. One source of systematic uncertainty is included specifically in the upper limits through the τ parameter, while the other sources of systematic uncertainty were included using the technique outlined in [14]. Using this method, the increase, ΔU_n, in the Poisson upper limit on the estimate for the number of rare decay events is:

$$\Delta U_n = \frac{1}{2}\, U_{\mathrm{RL}}^2\, \sigma_r^2\, \frac{U_{\mathrm{RL}} + b - n}{U_{\mathrm{RL}} + b} \tag{5}$$

where U_{RL} represents the Rolke-Lopez 90% confidence upper limit for the mean number of signal events, Y_{rare}, b is the predicted background in the signal region, n is the number of events found in the signal region and the total relative systematic uncertainty is σ_r. For example, uncertainty in the normalizing branching ratios and efficiencies used in the calculation of the rare branching ratios is translated to a percent or relative error in the estimation of Y_{rare}.

The relative systematic uncertainty from the normalizing branching ratios, σ_{PDG}, comes from the PDG [16]. The relative systematic uncertainty stemming from the simulation of the data comes from the simulation of the experimental trigger, $\sigma_{\mathrm{Trigger}}$, and the estimation of the efficiency of the outer muon system, $\sigma_{\mu\mathrm{ID}}$. Since the FOCUS trigger requires a minimum energy be deposited in the calorimetry, muons and hadrons will deposit very different energies, and the trigger simulation must account for any difference. The difference between three very different simulations is used to estimate this uncertainty: a full GEANT [17] simulation of the calorimetry, a pre–stored shower library generated with GEANT which selects the calorimetry response based on particle types, energies, and locations, and a simulation based on the parameterized average response in data of the calorimetry based on incident particle types and energies. The relative systematic error due to the outer muon identification is estimated by looking at the difference in the Monte Carlo rare decay efficiency for 2 different estimations of the the outer muon identification efficiency. One method employs the overlap between the inner and outer systems (very parallel muons coming from far upstream of the experiment can impact both systems), and the other method uses 2 hits in the outer system to predict a third hit. The final source of systematic error is due to the uncertainty in the modelling of the muon misidentification used when τ is calculated for the $D^+ \to K^-\mu^+\mu^+$ decay mode. This uncertainty is estimated by boosting the contribution of $D^+ \to K^-\pi^+\pi^+$ in the photoproduction Monte Carlo by twice the amount needed to match the amount of $D^+ \to K^-\pi^+\pi^+$ seen when one

of the pions is misidentified by a muon. The more conservative τ is then used. The small statistical errors from the ratio of Monte Carlo efficiencies and the error in the yield of the normalization modes did not contribute significantly to the systematic error.

The sources of relative systematic error for each mode are shown in Table 2. The total relative systematic uncertainty is obtained by adding all the contributions in quadrature. The effect on the rare branching ratio is calculated for each bootstrap sample and is naturally included in the ensemble result.

Table 2
Contributions to the relative systematic uncertainty, σ_r, in %.

Decay Mode	σ_{Trigger}	$\sigma_{\mu\text{ID}}$	σ_{PDG}	σ_r
$D^+ \to K^+\mu^+\mu^-$	2.8	1.9	6.7	7.5
$D^+ \to K^-\mu^+\mu^+$	2.7	2.6	6.7	7.7
$D^+ \to \pi^+\mu^+\mu^-$	2.5	2.7	6.7	7.6
$D^+ \to \pi^-\mu^+\mu^+$	2.0	2.6	6.7	7.5
$D_s^+ \to K^+\mu^+\mu^-$	3.0	1.9	27.3	27.5
$D_s^+ \to K^-\mu^+\mu^+$	2.3	2.5	27.3	27.5
$D_s^+ \to \pi^+\mu^+\mu^-$	3.6	2.7	27.3	27.7
$D_s^+ \to \pi^-\mu^+\mu^+$	3.0	2.8	27.3	27.6

To compare the Dual Bootstrap results to a more traditional "blind" analysis, another technique was used that selected a unique set of cuts, or point on the cut grid. Since the D^+ and D_s^+ lifetimes and production topology differ, a separate point on the cut grid was determined for each. The cuts used to determine the best sensitivities in the first bootstrap are saved for all four rare modes of a parent particle. A point in the multi-dimensional cut grid is determined by choosing cuts closest to the average value of each saved cut (see Figure 4). The cuts represented by these 2 cut grid points, one for the D^+ and one for the D_s^+, are then applied to the respective modes *once* in the spirit of a more traditional "blind" analysis. A branching ratio limit is computed using the resultant data histogram and the previous definitions for the signal region, the background sidebands, and τ. The best average cuts are shown in Table 1, and the data histograms resulting from this check are shown in Figures 5 and 6. A comparison was also made between the confidence limit calculated using the Rolke-Lopez method [15] and the Feldman–Cousins method [12]. Little difference was seen. We stress that these checks are provided as a convenience to the reader. As stated previously, the methods of Rolke and Lopez [11,15] have been demonstrated to provide correct coverage, whereas the coverage of the checks mentioned has either not been studied or, in the case of Feldman-Cousins where background fluctuations are not considered, has been shown to

be incorrect.

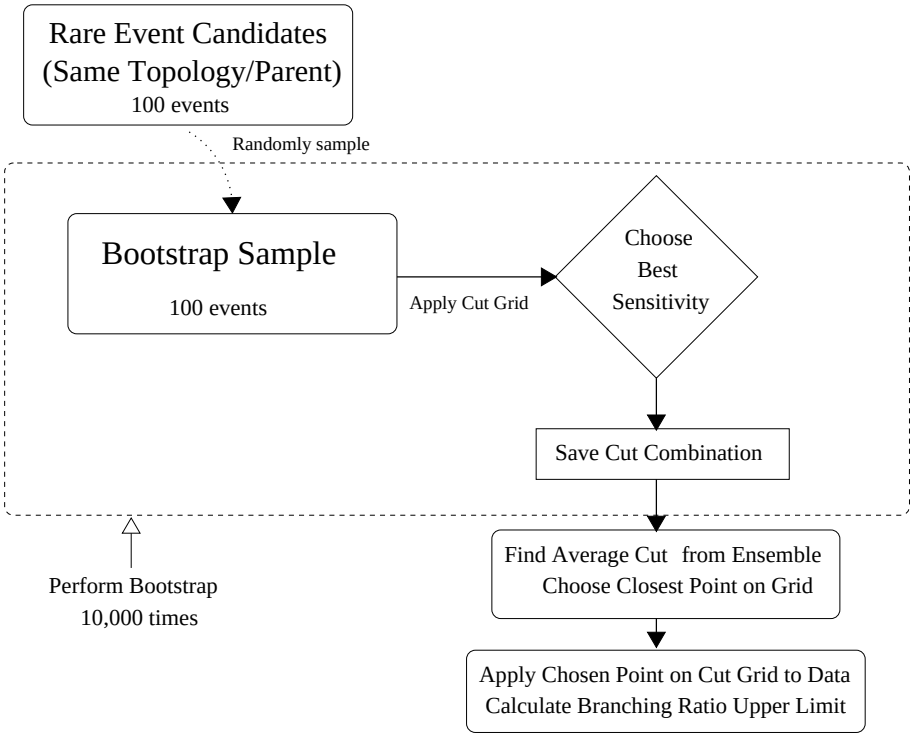

Fig. 4. A flowchart for the cut bootstrap on a sample size of 100 events. This figure should be compared to Figure 2. In this technique we determine an average "best cut" for the data using only the data sidebands and the expected shape of the background.

No significant evidence for the observation of any of the rare decay modes was seen. All modes except $D^+ \to K^-\mu^+\mu^+$ had a 90% lower limit for the branching ratio of zero. For $D^+ \to K^-\mu^+\mu^+$, the 96% lower limit was zero. The results of the analysis are presented in Table 3 below. There is good agreement between the Dual Bootstrap branching ratios (for both the Feldman-Cousins and Rolke-Lopez limits), the sensitivities, and the single cut systematic checks.

5 Summary and Conclusions

The FOCUS results from this analysis are shown in comparison to previous best results and recent theory in Table 4. Our results are a substantial improvement over previous results [4,5] and the FOCUS result for the branching ratio upper limit $D^+ \to \pi^+\mu^+\mu^-$ of 8.8×10^{-6} @ 90% C.L. is lower than the current MSSM R-Parity violating constraint [1] for this mode.

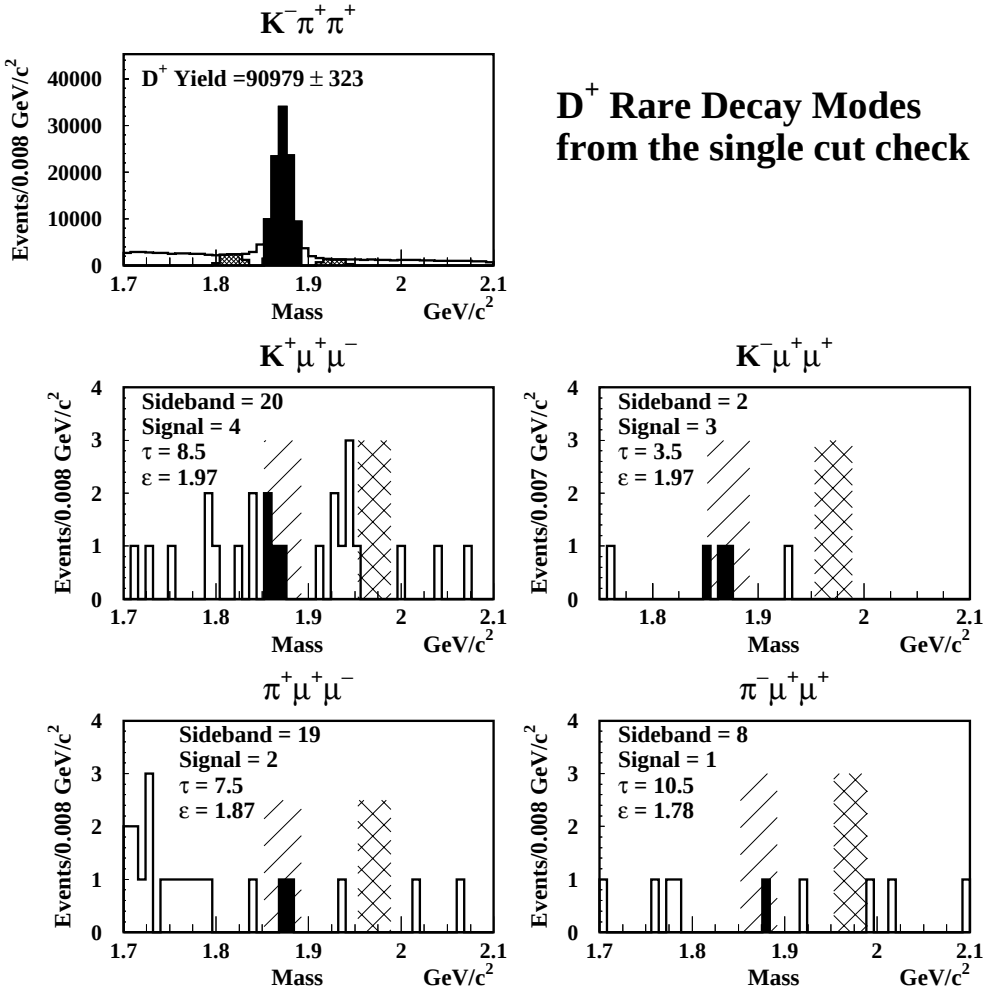

Fig. 5. Data used in the single cut systematic check for the D^+ decay modes. Note that the τ's shown on the plots are the same as those used for the Dual Bootstrap analysis. The solid histogram entries correspond to events in the signal region. The cross-hatched areas to either side of the normalization mode signal correspond to the data used for the sideband subtraction. The singly hatched areas in the di-muon mode histograms correspond to the signal region, while the cross-hatched areas correspond to an excluded region. All the other data and area shown in the di-muon histograms are used for the background estimate.

Acknowledgments

We wish to acknowledge the assistance of the staffs of Fermi National Accelerator Laboratory, the INFN of Italy, and the physics departments of the collaborating institutions. This research was supported in part by the U. S. National Science Foundation, the U. S. Department of Energy, the Italian Istituto Nazionale di Física Nucleare and Ministero dell'Università e della Ricerca

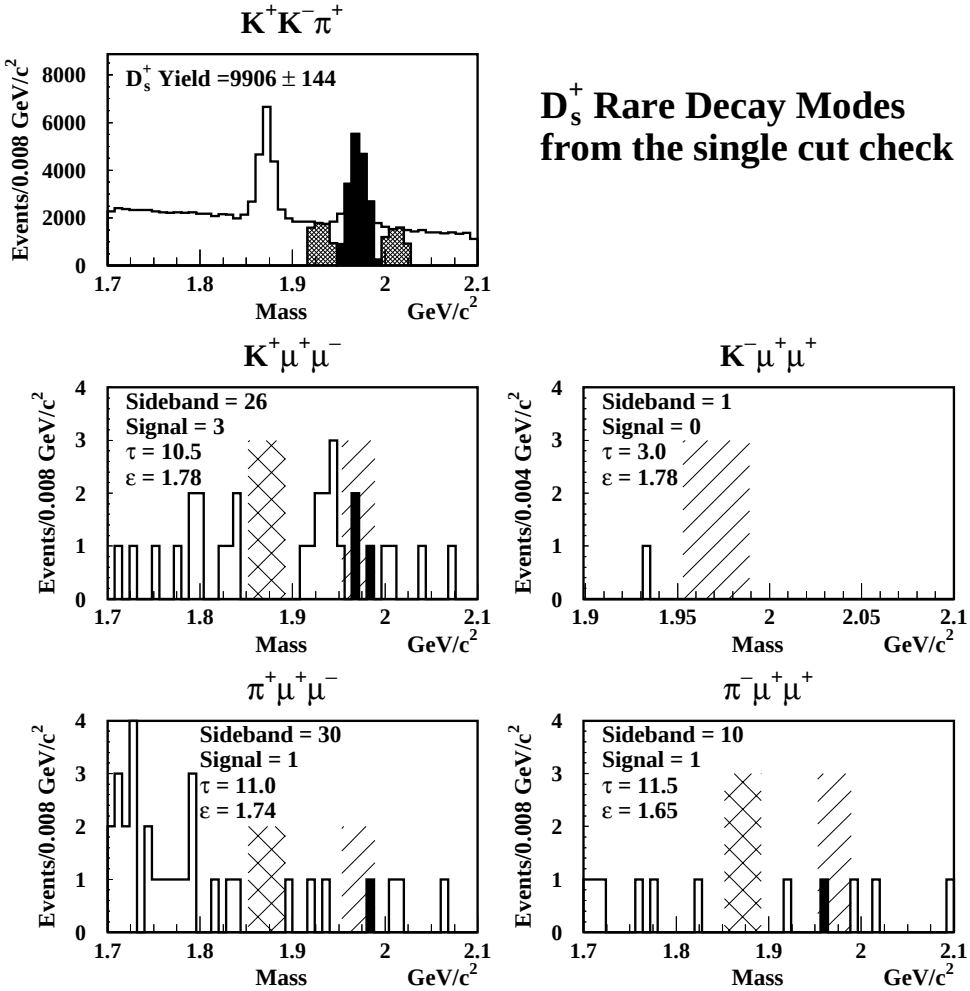

Fig. 6. Data used in the single cut systematic check for the D_s^+ decay modes. Note that the τ's shown on the plots are the same as those used for the Dual Bootstrap analysis. The solid histogram entries correspond to events in the signal region. The cross-hatched areas to either side of the normalization mode signal correspond to the data used for the sideband subtraction. The singly hatched areas in the di-muon mode histograms correspond to the signal region, while the cross-hatched areas correspond to an excluded region. All the other data and area shown in the di-muon histograms are used for the background estimate.

Scientifica e Tecnologica, the Brazilian Conselho Nacional de Desenvolvimento Científico e Tecnológico, CONACyT-México, the Korean Ministry of Education, and the Korean Science and Engineering Foundation. The authors wish to thank Gustavo Burdman and Paul Singer for their patience during several very useful conversations.

Table 3
FOCUS results with and without incorporated systematic errors for the modes shown. Each number represents a 90% confidence upper limit for the brancing ratio of the decay mode listed. F-C represents the Feldman-Cousins 90% confidence upper limit. R-L represents the Rolke-Lopez 90% confidence upper limit. Note the relatively minor differences between the sensitivities, the Feldman-Cousins limits and the Rolke-Lopez limits. Our final result is the Rolke-Lopez 90% confidence upper limit including the systematic error shown in the fifth column of the table. The single cut check result, which also includes the systematic error, shown in the last column of the table, agrees with our final result as well. All modes are ($\times 10^{-6}$).

Decay Mode	Sensitivity	F-C	R-L	**R-L incl. σ_r**	Single Cut incl. σ_r
$D^+ \to K^+\mu^+\mu^-$	7.5	11	9.1	9.2	12
$D^+ \to K^-\mu^+\mu^+$	4.8	13	13	13	12
$D^+ \to \pi^+\mu^+\mu^-$	7.6	9.3	8.7	8.8	7.4
$D^+ \to \pi^-\mu^+\mu^+$	5.5	4.6	4.8	4.8	5.1
$D_s^+ \to K^+\mu^+\mu^-$	33	31	33	36	38
$D_s^+ \to K^-\mu^+\mu^+$	21	11	13	13	20
$D_s^+ \to \pi^+\mu^+\mu^-$	31	20	24	26	18
$D_s^+ \to \pi^-\mu^+\mu^+$	23	29	26	29	22

References

[1] G. Burdman, E. Golowich, J. Hewett and S. Pakvasa, Phys. Rev. D **66**, 014009 (2002).

[2] S. Fajfer, S. Prelovsek and P. Singer, Phys. Rev. D **64**, 114009 (2001).

[3] P. Singer and D. X. Zhang, Phys. Rev. D **55**, 1127 (1997).

[4] P. L. Frabetti *et al.* [E687 Collaboration], Phys. Lett. B **398**, 239 (1997).

[5] E. M. Aitala *et al.* [E791 Collaboration], Phys. Lett. B **462**, 401 (1999).

[6] P. L. Frabetti *et al.*, Nucl. Instrum. Meth. A **329**, 62 (1993).

[7] P. L. Frabetti *et al.* [E687 Collaboration], Nucl. Instrum. Meth. A **320**, 519 (1992).

[8] J. M. Link *et al.* [FOCUS Collaboration], Nucl. Instrum. Meth. A **484**, 270 (2002).

[9] J. M. Link *et al.* [FOCUS Collaboration], arXiv:hep-ex/0204023.

[10] J. M. Link *et al.* [FOCUS Collaboration], Phys. Lett. B **535**, 43 (2002).

[11] W. A. Rolke and A. M. Lopez, Nucl. Instrum. Meth. A **503**, 617 (2003), and Proceedings of the Conference: Advanced Statistical Techniques in Particle Physics, Institute for Particle Physics Phenomenology, University of Durham, UK, 2002, 44-48.

[12] G. J. Feldman and R. D. Cousins, Phys. Rev. D **57**, 3873 (1998).

[13] F. James and R. Cousins, Eur. Phys. J. C **15**, 195 (2000).

[14] R. D. Cousins and V. L. Highland, Nucl. Instrum. Meth. A **320**, 331 (1992).

[15] W. A. Rolke and A. M. Lopez, Nucl. Instrum. Meth. A **458**, 745 (2001).

[16] D.E. Groom *et al.* [Particle Data Group Collaboration], Eur. Phys. J. C **15**, 1 (2000).

[17] GEANT, CERN Program Library Long Writeup W5013 (1993).

Table 4
FOCUS results compared to other experiments and recent theory. The previous limits, except for the E687 $D^+ \to K^-\mu^+\mu^+$ [4] are from Fermilab experiment E791 [5]. The theory estimates come from [2] (SM-1), [3] (SM-3), and [1] (R-Parity MSSM and SM-2). Note that the SM estimates from [1] use a formalism close to [3], and at present there is some discrepancy in the invariant M_{ll} mass behavior for the SM estimates in SM-3 [1] and SM-1 [2]. All modes shown are ($\times 10^{-6}$).

Decay Mode	This Analysis	SM-1	SM-2	SM-3	MSSM R-Parity	Previous Best
$D^+ \to K^+\mu^-\mu^+$	9.2	0.007	-	-	-	44
$D^+ \to K^-\mu^+\mu^+$	13	-	-	-	-	120
$D^+ \to \pi^+\mu^-\mu^+$	8.8	1.0	1.9	1.8	15	15
$D^+ \to \pi^-\mu^+\mu^+$	4.8	-	-	-	-	17
$D_s^+ \to K^+\mu^-\mu^+$	36	0.043	-	-	-	140
$D_s^+ \to K^-\mu^+\mu^+$	13	-	-	-	-	180
$D_s^+ \to \pi^+\mu^-\mu^+$	26	6.1	-	-	-	140
$D_s^+ \to \pi^-\mu^+\mu^+$	29	-	-	-	-	82